

# PCCP

Accepted Manuscript



This is an *Accepted Manuscript*, which has been through the Royal Society of Chemistry peer review process and has been accepted for publication.

*Accepted Manuscripts* are published online shortly after acceptance, before technical editing, formatting and proof reading. Using this free service, authors can make their results available to the community, in citable form, before we publish the edited article. We will replace this *Accepted Manuscript* with the edited and formatted *Advance Article* as soon as it is available.

You can find more information about *Accepted Manuscripts* in the [Information for Authors](#).

Please note that technical editing may introduce minor changes to the text and/or graphics, which may alter content. The journal's standard [Terms & Conditions](#) and the [Ethical guidelines](#) still apply. In no event shall the Royal Society of Chemistry be held responsible for any errors or omissions in this *Accepted Manuscript* or any consequences arising from the use of any information it contains.



## Photocatalytic reduction of triclosan on Au-Cu<sub>2</sub>O nanowire arrays as plasmonic photocatalysts under visible light irradiation†

Junfeng Niu,<sup>a</sup> Yunrong Dai,<sup>a</sup> Lifeng Yin,<sup>a</sup> Jianying Shang<sup>b</sup> and John C. Crittenden<sup>c</sup>

Received 00th January 20xx,  
Accepted 00th January 20xx

DOI: 10.1039/x0xx00000x

www.rsc.org/

Triclosan (TCS) is potentially threatening the environment and human health. Photocatalysis can be used to degrade TCS, but the photocatalytic efficiency is usually limited by the photoabsorptivity and photostability of the photocatalyst. In addition, some toxic by-products might also be generated during photocatalytic processes. In this study, we prepared Au-coated Cu<sub>2</sub>O nanowire arrays (Au-Cu<sub>2</sub>O NWAs) by beam sputtering Au onto Cu<sub>2</sub>O nanowires grown from a Cu foil. We found that photocatalytic degradation of TCS under visible light (420 nm <  $\lambda$  < 780 nm) irradiation and Au-Cu<sub>2</sub>O NWAs had several advantages. Au-Cu<sub>2</sub>O NWAs had good photoabsorptivity, high photostability (negligible activity loss after 16 runs), excellent photocatalytic activity (47.6 times faster than that of Cu<sub>2</sub>O), and low dichlorodibenzo-dioxins/dichlorohydroxydibenzofurans yield. The degradation intermediates were identified as chlorophenoxyphenols, phenoxyphenol, chlorophenol, catechol, phenol, benzoquinone, and lower volatile acids. We developed the degradation pathway of TCS mechanism which follows electron reduction and then oxidation by reactive oxygen species. The mechanism was developed and solidified using the radicals trapping and measurements. The unusual mechanism and photostability of Au-Cu<sub>2</sub>O NWAs were attributed to the Au/Cu<sub>2</sub>O/Cu “sandwich” like structure. This structure yields a sustained and steady internal electric field, raises the conduction band of Cu<sub>2</sub>O, reinforces the reductive activity of the photo-generated electrons, and eliminates the photo-generated holes that are responsible for the photo-etching of Cu<sub>2</sub>O.

### 1. Introduction

Triclosan (2,4,4'-trichloro-2'-hydroxydiphenyl ether; TCS) is a synthetic, non-ionic, broad-spectrum antimicrobial compound that is widely used in health care products and personal consumer products, such as toothpastes, soaps, shampoos, textiles and plastics.<sup>1</sup> Various concentrations of TCS ranging from 35 ng L<sup>-1</sup> to 10  $\mu$ g L<sup>-1</sup> have been detected in freshwater,<sup>2</sup> seawater<sup>3</sup>, and wastewater.<sup>4</sup> TCS, with accumulation and long-term persistence in the environment, potentially resulted in acute cytotoxicity or chronic genotoxicity for aquatic organisms, such as mussels,<sup>5</sup> insects,<sup>6</sup> and fishes.<sup>7</sup> Recently, USA Environmental Protection Agency (EPA) has suggested that TCS potentially affects human health, and started to conduct a review of TCS.<sup>8</sup> USA Food and Drug Administration (FDA) also agreed to set a regulation for TCS.<sup>9</sup>

To avoid further accumulation of TCS in water, the removal of TCS attracts increasing attention. TCS can be partially removed by conventional wastewater<sup>10</sup> and drinking water

treatment, however, complete removal of TCS is not achieved.<sup>11</sup> Recently, some techniques, including electrocatalysis,<sup>12</sup> Fenton oxidation,<sup>13</sup> electrolysis and sonoelectrolysis<sup>14</sup> have been applied to treat TCS. Some of these techniques have resulted in partial degradation or generation of toxic by-products.<sup>15</sup> Several research groups are utilizing UV-photocatalysis, an advanced oxidation process (AOP) where hydroxyl radicals ( $\cdot$ OH) are generated to degrade TCS in water.<sup>16</sup> However, UV-light transforms TCS into toxic chlorinated dioxins, such as 2,7/2,8-dichlorodibenzo-dioxins (DCDDs).<sup>17,18</sup> Moreover, only 4–6% of sunlight energy can be used by UV-photocatalysis.<sup>19</sup> If artificial light resources are used, the energy cost will be significant. Accordingly, visible light driven photocatalysis is an attractive alternative to remove TCS from water.<sup>20</sup> Because the absorption spectrum of TCS is in the UV range, there is little chance for TCS to be transformed to chlorinated dioxins using visible light irradiation. Although it has not been reported to our knowledge.

Cuprous oxide (Cu<sub>2</sub>O) is a visible light driven photocatalyst that has been investigated for water splitting,<sup>21,22</sup> CO<sub>2</sub> reduction,<sup>23–25</sup> organic synthesis<sup>26</sup> and the removal of pollutants<sup>27,28</sup> for a long time. Compared with traditional semiconductor photocatalysts, such as TiO<sub>2</sub> and ZnO, Cu<sub>2</sub>O has a larger photoabsorptivity, quantum yield and energy utilization efficiency.<sup>29</sup> However, the reductive and oxidative potentials of Cu<sub>2</sub>O (–1.28 V and +0.92 V, vs. NHE) do not produce hydroxyl radical.<sup>30</sup> Worse yet, Cu<sub>2</sub>O is easily deactivated by photo-etching after light irradiation for several

<sup>a</sup> State Key Laboratory of Water Environment Simulation, School of Environment, Beijing Normal University, Beijing 100875, P. R. China.

<sup>b</sup> State Key Laboratory of Environmental Criteria and Risk Assessment, Chinese Research Academy of Environmental Sciences, Beijing 100012, P. R. China.

<sup>c</sup> School of Civil and Environmental Engineering and the Brook Byers Institute for Sustainable Systems, Georgia Institute of Technology, Atlanta, GA 30332, United States.

† Electronic Supplementary Information (ESI) available: Complementary material for preparation, characterization, experimental test, calculations, and discussion on mechanism. See DOI: 10.1039/b000000x/

hours.<sup>31</sup> Therefore, Cu<sub>2</sub>O is seldom considered as a photocatalyst for large-scale environmental application. Recently, it has been reported that plasmonic nanostructure might reinforce the activity of photocatalyst under visible light irradiation.<sup>32</sup> Plasmonic photocatalysis makes use of noble metal nanoparticles dispersed into semiconductor photocatalysts, building a Schottky junction and forming localized surface plasmonic resonance (LSPR), by which charge separation is enhanced and more active charge carriers are excited. Based on these findings, some Au-Cu<sub>2</sub>O composite nanostructures<sup>33,34</sup> were developed and proved to be upgraded on their photocatalytic performance.

In this study, we performed a simple thermal evaporation approach to prepare Cu<sub>2</sub>O nanowire arrays (Cu<sub>2</sub>O NWAs) and sputtered Au on them. We intended to show that the mass production of Au coated Cu<sub>2</sub>O nanowire arrays (Au-Cu<sub>2</sub>O NWAs) could be achieved and reduce Cu<sub>2</sub>O photo-etching. The Au-Cu<sub>2</sub>O NWAs were used for the photocatalytic degradation of TCS in water under visible light irradiation, and their photocatalytic activity and photostability were evaluated. Moreover, we proposed a detailed degradation pathway of TCS and evaluated the potential risk of its by-products. The mechanism of TCS degradation by the Au-Cu<sub>2</sub>O NWAs was also developed based on the photocatalytic reduction and the orientation of photo-generated electron carriers.

## 2. Experimental

### 2.1 Au-Cu<sub>2</sub>O NWAs preparation

A thermal annealing method<sup>35</sup> was used to synthesize Cu<sub>2</sub>O NWAs on Cu foils. This method was developed based on the previous reported synthesis of CuO NWAs.<sup>36,37</sup> A Cu foil (100×100 mm<sup>2</sup>, 0.5 mm in thickness) was polished and washed using dilute nitric acid (0.1 M) and absolute ethanol for 3–5 times, and then dried in the air. Next, the Cu foil was placed into a covered quartz crucible in air. A heating rate of 20°C min<sup>-1</sup> was used to increase the initial temperature from 250 to final temperature by a muffle furnace. We used 250, 350, 450 and 550°C for the final annealing temperature. After annealing at the final temperature for 120 min, the samples were cooled with atomized absolute ethanol. Next, the samples were placed in an IMS500 sputter coater (CAS instrument, China). Before coating, the sputtering chamber was evacuated to 5.0×10<sup>-4</sup> Pa. Then, an Au layer was deposited onto the samples after sputter coating for 30 s, and the Au-Cu<sub>2</sub>O NWAs were obtained (See *Supplementary Information*).

### 2.2 Characterization

The morphology and structure of the Au-Cu<sub>2</sub>O NWAs were observed with a Hitachi S-4800 (Japan) field emission scanning electron microscope (FESEM), equipped with an energy dispersive X-ray spectrometer (EDS) for detecting the element composition. A double monochromator (JobinYvon-U1000, France) equipped with a photoncounting system was used to conduct Raman analysis. The samples were excited at 514.5 nm (2.41 eV) with an argon laser in a backward configuration.

Powder X-ray diffraction (XRD) patterns of the samples were recorded using an X'Pert PRO MPD diffractometer (PANalytical, Netherland) with a source of Cu-K $\alpha$  radiation ( $\lambda=0.15418$  nm). The work functions were measured by ultraviolet photoelectron spectroscopy (UPS) on an Axis Ultra instrument (Kratos, Japan). Diffuse reflectance spectrophotometry (DRS) was performed using a Cary 500 UV-vis spectrophotometer (Varian, USA) with an integrating sphere attachment in the range of 200–1000 nm. Detailed photoelectrochemical measurements are described in *Supplementary Information*.

### 2.3 Photocatalytic experiments

Cu<sub>2</sub>O NWAs and Au-Cu<sub>2</sub>O NWAs were used as photocatalysts. For batch experiments (see Fig. S1<sup>†</sup>), the Cu NWAs were cut into wafers with a diameter of 80 mm, and then placed in the bottom of the glass culture dish (diameter 90 mm). Next, 100 mL of 5.0 mg L<sup>-1</sup> TCS solution was added into the culture dish which resulted in a solution depth of 20 mm. Then the culture dish was put on a shaker (30 rpm, 25±1°C) for 30 min in the dark. For the photocatalytic experiments, a Xenon lamp (CHF-XM-500W; Trusttech, China) with a SCF-S50-42L cut-off filter was placed 100 mm above the solution. The concentration of TCS was measured by means of high performance liquid chromatography (HPLC, Dionex U-3000, USA) with a UV detector set at 280 nm. The concentration of chloride ions was measured by ion chromatography (IC, Dionex ICS-900, USA). The total organic carbon (TOC) of samples was measured on a Shimadzu TOC-VCSH analyzer (Japan). To compare the difference between visible light driven photocatalysis and UV-photocatalysis, the experiments were also conducted in the same reactors under low-pressure mercury lamp (dominant wavelength 365 nm, Philips TLD15W/05, Netherland) irradiation. The light intensity in the center of the reaction solution was 5.2 × 10<sup>-9</sup> Einstein cm<sup>-2</sup> s<sup>-1</sup>. Intensity of illumination is 326  $\mu$ W cm<sup>-2</sup>. As a control, the degradation of TCS by 0.5 g of TiO<sub>2</sub> nanoparticles (TiO<sub>2</sub> NPs, Degussa, Germany) was also investigated under the same conditions.

### 2.4 Identification of intermediates

A triple-stage quadrupole mass spectrometer (API3200, Applied Biosystems, USA) coupled with HPLC (LC-MS) was used to identify the photochemical intermediates. Either a Varian Pursuit 5-C18 or an Inertsil 5 ODS-3 column was used for separation. On the Pursuit column, a linear gradient of methanol and acetic acid aqueous solution (1.5 %, v/v) increasing from a ratio of 50:50 to 100:0 at a flow rate of 0.5 mL min<sup>-1</sup> was used to separate TCS and its intermediates, except for acids. The total analysis time was 30 min. On the ODS-3 column, water and acetonitrile at a ratio of 30:70 were used to separate the intermediates of acids. The electrospray ionization (ESI) source was operated in negative mode.

To verify the results of LC-MS, the same aqueous samples was extracted with equal volume of n-hexane and analyzed by an Agilent 7890/5975 GC-MS (USA), equipped with a J&W DB-5 fused-silica capillary column (30 m × 0.25 mm). Pure helium

was used as the carrier gas with a flow rate at  $1.0 \text{ mL min}^{-1}$ . The oven program was initially at  $100 \text{ }^\circ\text{C}$  (hold for 0.5 min), then increased at  $5 \text{ }^\circ\text{C min}^{-1}$  to  $250 \text{ }^\circ\text{C}$  (hold for 2 min). The electron energy was set at 70 eV and the ion source temperature at  $230 \text{ }^\circ\text{C}$ . To detect the trace by-products, including DCDDs and dichlorohydroxydibenzofurans (DCHDFs), the reaction solution (after 30 min irradiation) were concentrated using solid-phase extraction (SPE) column (Waters Sep-Pak C18, USA) and analyzed on GC-MS-SIM (selected ion monitoring) using the same program.

### 2.5 Reactive radical trapping

To determine the reactive radicals involved in the photocatalytic degradation of TCS by the Au-Cu<sub>2</sub>O NWAs, three selective radical trappers, including formic acid, sodium azide, and hydrogen peroxide, were used to measure  $\cdot\text{OH}$ , singlet oxygen ( $^1\text{O}_2$ )/superoxide radical ( $\cdot\text{O}_2^-$ ), and electrons, respectively. Other experimental conditions were same with those described in "Photocatalytic Experiments" section. The TCS concentration was measured using HPLC. The radicals concentrations were also measure by electron spin resonance (ESR) using a Bruker ESP-300E ESR spectrometer equipped with a quanta-Ray NdYAG laser system. (detailed operation conditions are described in the *Supplementary Information*).

## 3. Results and discussion

### 3.1 Morphology and composition

The SEM images and EDS spectra of Cu foils under different annealing temperatures were analyzed. As seen from Fig. S2 and S3†, under the annealing temperature of  $250^\circ\text{C}$  and  $350^\circ\text{C}$ , the thermal evaporation covered the Cu foil with a mass of particles, and the atomic ratios of Cu and O were 1.02:1 and 1.54:1 identified on the EDS patterns. When the annealing temperature was increased to  $450^\circ\text{C}$ , the abundant nanowires were successfully grown on the Cu foil and formed NWAs, as shown in Fig. 1. The nanowires were high-quality and uniformly distributed, with lengths over  $5 \mu\text{m}$ , aspect ratios up to 45. The formation of these nanowires might be explained by that the adsorbed species progressively acquired a higher surface mobility with the increase of the annealing temperature, resulting ultimately in the observed anisotropic structures.<sup>38</sup> Meanwhile, the atomic ratio of Cu and O rose with the increase of the annealing temperature and finally reached 1.98:1 (Fig. S3(c)†), which indicated the possible formation of Cu<sub>2</sub>O. Although relatively high annealing temperature ( $550^\circ\text{C}$ ) might lead to the formation of Cu<sub>2</sub>O (Cu:O=1.99:1), it also resulted in the transformation of the sample morphology from nanowires to the larger micro-scale prisms (Fig. S2(c)†). On the EDS patterns (Fig. S3†), trace amount of coated Au atoms can be identified, but cannot be well quantified, which might be due to the low content of Au (<1%). Therefore, the annealing temperature of  $450^\circ\text{C}$  was considered as the optimal condition for prepare the Au-Cu<sub>2</sub>O NWAs in this study.

Raman spectra are further investigated for Cu<sub>2</sub>O NWAs with/without Au coating. As shown in Fig. 1c, the peaks of Cu<sub>2</sub>O NWAs are found at  $225 \text{ cm}^{-1}$  ( $2\Gamma_{12}^-$ , vibration mode),  $318 \text{ cm}^{-1}$  ( $2\Gamma_{12}^-$ ),  $412 \text{ cm}^{-1}$  ( $\Gamma_{15}^-$ ), and  $624 \text{ cm}^{-1}$  ( $\Gamma_{15}^-$ ),<sup>39</sup> indicating the cubic cuprite domination. For Au-Cu<sub>2</sub>O NWAs, a new band appears at  $102 \text{ cm}^{-1}$  ( $2\Gamma_{12}^-$ ), while the intensities of the  $2\Gamma_{12}^-$  modes at  $225 \text{ cm}^{-1}$  and  $318 \text{ cm}^{-1}$  exhibit a significant increase, suggesting the enhancement by plasma resonance.

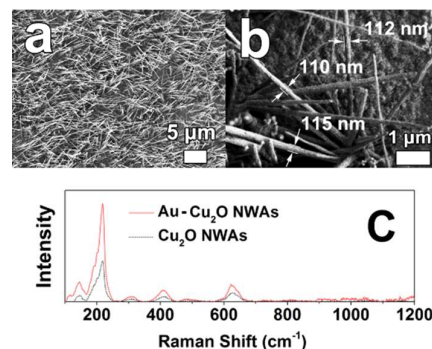


**Fig. 1.** Scanning electron microscope images of the Cu foil annealed at  $450^\circ\text{C}$

XRD analysis provided an additional confirmation of the pure Cu<sub>2</sub>O phase. As shown in Fig. S4(a)† and (b), the XRD patterns of the samples collected by scraping the surface layer of the Cu foils annealed at  $450^\circ\text{C}$ . We can clearly see that both samples (Cu<sub>2</sub>O NWAs and Au-Cu<sub>2</sub>O NWAs) can be characterized as a cubic Cu<sub>2</sub>O phase with a lattice constant of  $a=0.4252 \text{ nm}$  (JCPDS: 1-1142). In addition, no other phase, such as CuO and Cu, can be observed. The results also indicate that the Cu<sub>2</sub>O NWAs synthesized by thermal evaporation have relatively high percentage of (111) facets.

DRS was used to characterize the photoabsorptivity of the as-prepared Au-Cu<sub>2</sub>O NWAs. Fig. S6† shows that the Au-Cu<sub>2</sub>O NWAs exhibited an obvious red shift compared to the Cu<sub>2</sub>O NWAs. This red shift indicated that the Au coating extended the photoabsorption edge into long-wavelength visible light region. The photoabsorption is aligned well with the solar spectrum (See *Supplementary Information*, "Photoabsorptivity"). Accordingly, Au-Cu<sub>2</sub>O NWAs can take full advantage of visible light energy in sunlight.

### 3.2 Removal of TCS

Fig. 2 shows the destruction of TCS using the Cu<sub>2</sub>O NWAs and Au-Cu<sub>2</sub>O NWAs under visible light irradiation ( $>420 \text{ nm}$ ). Prior to the first run, the concentration of TCS solution slightly decreased when it was stored in dark, due to the adsorption of TCS by the NWAs. During the first run, the half-hour removal efficiency of TCS by the Au-Cu<sub>2</sub>O NWAs was 5 times that of Cu<sub>2</sub>O NWAs ( $98.6\pm 0.5\%$  vs.  $17.9\pm 0.7\%$ ). Both reactions followed pseudo-first order kinetics and the rate constants were  $0.238$  and  $0.005 \text{ min}^{-1}$ , for the Au-Cu<sub>2</sub>O NWAs and Cu<sub>2</sub>O NWAs, respectively (see *Supplementary Information*, "Kinetics").

During the reaction, the pH value of solution was slightly decreased from 7.4 to 6.5, suggesting the dechlorination and the yield of little HCl. Furthermore, the dechlorination process was confirmed by measuring the concentration change of Cl<sup>-</sup> ions. It was also found that the amount of Cl<sup>-</sup> was positively related to the degradation of TCS. Chlorinated groups are the primary toxicity source of TCS; therefore, the photocatalytic dechlorination might detoxify TCS and reduce its potential environmental risk. However, the TOC concentrations changed slightly during the entire reaction, suggesting that only small amount of TCS was mineralized by the Au-Cu<sub>2</sub>O NWAs.

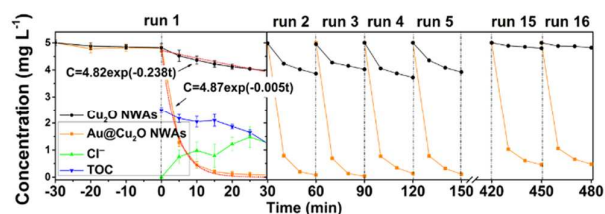


**Fig. 2.** TCS concentration changes during the photocatalytic degradation by Cu<sub>2</sub>O NWAs and Au-Cu<sub>2</sub>O NWAs in single and recycled tests (30 rpm, 25±1 °C) under visible light (>420 nm) irradiation. The time courses in runs 6–14 were omitted. TOC and Cl<sup>-</sup> concentration changes during the photocatalytic degradation by Au-Cu<sub>2</sub>O NWAs were also presented.

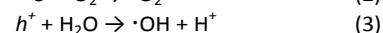
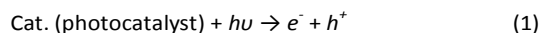
For evaluate the stability of Au-Cu<sub>2</sub>O NWAs, the reaction solution was evacuated and the fresh TCS solution was added. This process was repeated 16 times. In the first four runs, the removal efficiencies of TCS did not significantly decrease, and the average removal efficiencies by the Cu<sub>2</sub>O NWAs and Au-Cu<sub>2</sub>O NWAs were 23.2% and 96.5%, respectively. After thirteen runs, the photocatalytic activity of the Cu<sub>2</sub>O NWAs was obviously inhibited, and the removal efficiency decreased from 21.2% to 0.97%. By contrast, the Au-Cu<sub>2</sub>O NWAs still maintained their high activity, with a removal efficiency as high as 95.0%.

### 3.3 Oxidation or reduction?

During the photocatalytic experiment, the Au-Cu<sub>2</sub>O NWAs exhibited impressive photocatalytic activity and photostability compared with the Cu<sub>2</sub>O NWAs. However, the high photostability and low TOC removal efficiency implied a distinctive photocatalytic pathway in contrast with traditional photocatalytic oxidation studies using Cu<sub>2</sub>O.<sup>40</sup> This special phenomenon encouraged us to clarify the detailed mechanism of TCS degradation using Au-Cu<sub>2</sub>O NWAs.

Firstly, which reactive radicals played the major role in the degradation of TCS should be determined. When light beam strikes a photocatalyst, it excites electrons out of the valence band (VB) and create holes in the VB (Equation 1). The electrons which have moved up to the conduction band (CB) can migrate to the catalyst surface and react with oxygen molecules to generate ·O<sub>2</sub><sup>-</sup> (Equation 2). The holes can oxidize

water into ·OH (Equation 3)<sup>41</sup> if they have sufficient oxidation potential and can oxidize ·O<sub>2</sub><sup>-</sup> into <sup>1</sup>O<sub>2</sub> (Equation 4).<sup>42</sup>



In the aqueous solution, those reactive oxygen species (ROS, including ·OH, ·O<sub>2</sub><sup>-</sup>, and <sup>1</sup>O<sub>2</sub>) are reduced by electron donors. Electrons also react with electron acceptors. Therefore, electron donors can act as radical trappers to inactivate ROS and restrain oxidative reactions, while maintain more electrons and enhance reductive reactions during a photocatalytic reaction. On the contrary, the electron acceptors can restrain the reductive reaction and enhances the oxidative reaction.<sup>43</sup>

The effects of radical trappers on the photocatalytic degradation of TCS by the Au-Cu<sub>2</sub>O NWAs are shown in Fig. 3. Here, formic acid,<sup>44</sup> sodium azide,<sup>45,46</sup> and hydrogen peroxide<sup>47</sup> were used as the radical trappers for ·OH, <sup>1</sup>O<sub>2</sub> (or ·O<sub>2</sub><sup>-</sup>), and electrons, respectively. Adding 26.0–55.0 mmol formic acid reinforced the activity of Au-Cu<sub>2</sub>O NWAs and degradation of TCS; adding 2.0–4.0 mmol sodium azide also improved the degradation efficiency of TCS, which indicated that ·OH, <sup>1</sup>O<sub>2</sub> (or ·O<sub>2</sub><sup>-</sup>) were not the main active species involved in these reactions. And their formation is not the rate-limiting step of TCS degradation (the absence of ·OH and <sup>1</sup>O<sub>2</sub> was also verified by ESR analysis, see *Supplementary Information*). By contrast, adding 4.0–8.0 mmol hydrogen peroxide, which acted as an electron trapper, diminished the degradation of TCS, indicating that reduction by electrons play a predominant role in the photocatalytic degradation of TCS by the Au-Cu<sub>2</sub>O NWAs.

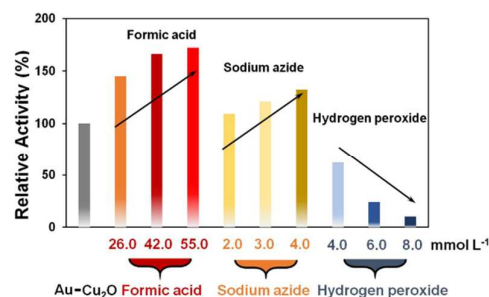


**Fig. 3.** Effects of radical trappers (formic acid, sodium azide, and hydrogen peroxide) on the degradation efficiency of TCS on the Au-Cu<sub>2</sub>O NWAs in aqueous solution.

Secondly, the photoelectrochemical measurement verified the stronger electron donating capacity of the Au-Cu<sub>2</sub>O NWAs than that of Cu<sub>2</sub>O NWAs. Fig. S13<sup>†</sup> illustrates the intermittent photocurrent of the Cu<sub>2</sub>O NWAs and Au-Cu<sub>2</sub>O NWAs measured under visible light irradiation (>420 nm). The samples were alternately irradiated and sheltered every 45 s. The maximum photocurrent of the Au-Cu<sub>2</sub>O NWAs was much stronger than that of Cu<sub>2</sub>O NWAs (-11.8 μA vs. -5.9 μA), suggesting the efficient separation of photo-generated electrons and holes in

the Au-Cu<sub>2</sub>O NWAs, thus enabling more electrons to react with electron acceptors (TCS) in solution.<sup>48</sup>

As shown in Fig. 4, the identification of the intermediates directly showed the presence of photocatalytic reduction during the degradation of TCS. The identification of primary degradation products allowed us to propose the reaction pathway for the transformation of TCS. In our case, TCS (I) was dechlorinated firstly and transformed into dichlorophenoxyphenol (II), which was identified as the initial product. Based on the analysis of radical trapping, the dechlorination might be attributed to the nucleophilic attack by electrons. According to the Frontier Molecular Orbit (FMO) calculation (see *Supplementary Information* and Fig. S14†), TCS was prone to be chlorinated on C2 site, rather than that on C4 or C4'. Compared with the photocatalytic oxidation routes of TCS, 2-chloro-5-(2,4-dichlorophenoxy)-[1,4] benzoquinone and 2-chloro-5-(2,4-dichlorophenoxy)-[1,4] hydroquinone<sup>49</sup> were not detected in our experiments, suggesting that little oxidation occurred in the first step. Sequentially, dichlorophenoxyphenol (II) was further dechlorinated into monochlorophenoxyphenol (III) and phenoxyphenol (IV), the ether linkage of which was cleaved and transformed into chlorophenol (V), catechol (VI), and phenol (VII). Meanwhile, the chlorophenol (V) might be further dechlorinated into phenol (VII). These phenolic products (VI and VII) were more easy to be oxidized rather than reduced. Because the photocatalytic reduction donated abundant photo-generated electrons, O<sub>2</sub><sup>-</sup> is more likely to be the major oxidative specie (see Equation 2). As a consequence, O<sub>2</sub><sup>-</sup> reacted with phenolic products (VI and VII) and generated semiquinone (VIII) and benzoquinone (IX), eventually leading to the formation of low molecular acids (X), including muconic acid, acetic acid, and oxalic acid.

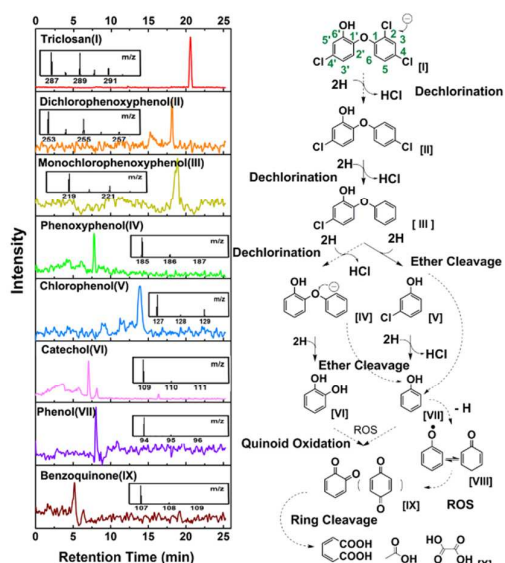


**Fig. 4.** Intermediates identified by LC-MS on C18 column (verified by GC-MS) and the proposed reaction pathway. All products are listed in the order they appeared in the photocatalytic reaction, and verified by their mass spectra and

authentic standards. Small molecular acids were separated on ODS-3 column.

These analyses show that reaction pathway would not be started unless reductive species existed<sup>50</sup>. ROS also played a key role during the follow-up oxidation of dechlorinated products. Combined with the results of radical trapping experiments, the transformation of TCS was driven first by the reductive dechlorination, and then by ROS oxidation. Herein, we have demonstrated that photocatalytic reduction dominated the initial destruction reactions then photocatalytic oxidation takes place.

### 3.4 Identification of DCDDs and DCHDFs

Under UV-light irradiation, TCS is degraded by photolysis or photocatalysis.<sup>51</sup> However, it has been demonstrated that DCDDs and DCHDFs, a class of compounds known to be toxic and carcinogenic, were generated during these degradation processes.<sup>52</sup> To investigate the generation of DCDDs and DCHDFs in our experiments, GC-MS-SIM was used to monitor for these compounds during photolysis or photocatalysis, under UV-light or visible light irradiation. As shown in Fig. S15(a-c)†, the peak at retention time 20.9 min belonged to the ions of TCS ( $m/z=288$  and  $m/z=290$ , in Fig. S15(d)†), which has been compared with an authentic standard. After UV-photolysis, TCS was degraded into two groups of products with peaks appeared at 18.4 min and 21.2 min (Fig. S15(a)†). The first of them can be identified as 2,7/2,8-DCDDs on the basis of authentic standard and the mass spectrum (Fig. S15(e)†). The base peak ions are  $m/z=252$  and  $m/z=254$ , corresponding to the molecular ions  $[M]^+$  and  $[M+2]^+$ , respectively. The similar mass spectra were also reported by previous studies.<sup>53</sup> However, the peaks at 21.2 min were difficult to confirm because they shared the similar mass spectra with 2,7/2,8-DCDDs. Considering the delayed retention time, we believed that DCHDFs were formed by the photo-induced dechlorination and cyclization of TCS.<sup>54</sup> By contrast, no DCDDs or DCHDFs was detected and little TCS was degraded under visible light irradiation, suggesting the photolysis of TCS could be negligible in this process.

In the presence of a TiO<sub>2</sub> nanoparticle (NP) photocatalyst, the degradation of TCS was significant under UV-light irradiation (Fig. S15(b)†). However, the toxic by-products, DCDDs and DCHDFs, were generated as well. The yield of DCDDs was even higher than that by UV-photolysis, which could be due to the  $\cdot\text{OH}$  oxidation and cyclization of TCS.<sup>55</sup> We also used the visible light and the TiO<sub>2</sub> nanoparticle photocatalyst, and found that TCS could not be degraded. Therefore, it is difficult to balance the toxicity reduction by TCS destruction and by product formation using TiO<sub>2</sub> photocatalysis.

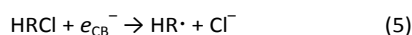
In the presence of Au-Cu<sub>2</sub>O NWAs, almost all of TCS was degraded under UV-light irradiation (Fig. S15(c)†), just like the photocatalytic degradation by TiO<sub>2</sub> NPs. However, the yield of DCDDs was dramatically diminished with a slight rise of

DCHDFs. Under visible light irradiation, better yet, none of toxic by-products, DCDDs or DCHDFs, were found.

Generally, two conditions need to be satisfied for the formation of DCDDs and DCHDFs. First,  $\cdot\text{OH}$  radicals are present for the cleavage and oxidation. Second, the chlorinated phenoxyphenols are not be dechlorinated into phenoxyphenols before they react with  $\cdot\text{OH}$ . We did not detect any  $\cdot\text{OH}$  in our work on visible light photolysis. And TCS and chlorinated phenoxyphenols were rapidly dechlorinated by photocatalytic reduction, and no longer acted as the precursor of DCDDs and DCHDFs. Therefore, it is safe to say that there was little chance for such a photocatalytic reduction process to produce DCDDs and DCHDFs using visible light photocatalysis. The visible light driven Au-Cu<sub>2</sub>O NWAs photocatalytic reduction can be safely used in the removal of TCS from water, and it does not produce the toxic by-products (DCDDs and DCHDFs).

### 3.5 Mechanism of photocatalytic reduction

Under light irradiation, a photocatalyst generates reductive electrons in CB ( $e_{\text{CB}}^-$ ) and oxidative holes in VB ( $h_{\text{VB}}^+$ ).<sup>55</sup> The degradation of chlorinated compound by photocatalysis can be initiated by either  $e_{\text{CB}}^-$  or  $h_{\text{VB}}^+$  when the redox reactions are thermodynamically favorable:<sup>50</sup>



For the Cu<sub>2</sub>O photocatalyst, the redox potential of  $e_{\text{CB}}^-$  is not sufficiently negative to be a versatile reducing agent.<sup>56</sup> So, why did photocatalytic reduction play a major role in the degradation of TCS by the Au-Cu<sub>2</sub>O NWAs? Is it related to the Au coating on the Cu<sub>2</sub>O NWAs? The underlying photocatalytic mechanism requires further investigation.

To track the energy band changes of Au, Cu<sub>2</sub>O, and Cu, their work functions under different conditions were measured by UPS (see Fig. S17†). The cutoff energy ( $E_{\text{cutoff}}$ ) and Fermi energy ( $E_{\text{Fermi}}$ ) are determined by linear extrapolation to the zero of the profiles. The work function can be calculated from using the Equation 7:<sup>57,58</sup>

$$\Phi = h\nu - E_{\text{cutoff}} + E_{\text{Fermi}} \quad (7)$$

where  $h\nu$  ( $=21.22$  eV) is the incoming photon energy from He I source;  $E_{\text{cutoff}}$  is the energy of cutoff edge;  $E_{\text{Fermi}}$  is the energy at Fermi energy level. As shown in Fig. S17(a)†, the  $E_{\text{cutoff}}$  of an Au nanoparticle and an Au nanoparticle that is coated on the Cu<sub>2</sub>O NWAs is 16.05 eV and 16.60 eV, respectively. And both of their  $E_{\text{Fermi}}$  are close to 0 eV. According to the Equation 7, the work function of an Au nanoparticle and an Au nanoparticle that is coated on the Cu<sub>2</sub>O NWAs are  $5.17 \pm 0.05$  eV and  $4.62 \pm 0.05$  eV, respectively. Thus, the Au nanoparticles show the lower work function (i.e. higher Fermi energy level) after coated onto the Cu<sub>2</sub>O NWAs. The electrons flow from the Cu<sub>2</sub>O side to CB of Au.

As shown in Fig. S17(b)†, the work function of Cu<sub>2</sub>O NWAs scraped from the Cu foil ( $5.06 \pm 0.05$  eV) is higher than that on Cu foil ( $4.67 \pm 0.05$  eV). However, the work function of Cu is

nearly identical ( $4.62 \pm 0.05$  eV), regardless whether NWAs are on it or not (see Fig. S17(c)†). Apparently, the electrons of Cu migrate into the energy band Cu<sub>2</sub>O after Cu<sub>2</sub>O/Cu contact.

In the Au/Cu<sub>2</sub>O/Cu “sandwich” like structure, the bulk Cu (Cu foil) might act as a pool of electrons. The work function of pure Cu foil is less than that of Au and Cu<sub>2</sub>O, resulting in abundant electrons in Cu transfer into the VB of Cu<sub>2</sub>O, and then into Au. This transfer builds a sustained and steady internal electric field, and raises both Fermi energy levels of Au and Cu<sub>2</sub>O (see Fig. 5b). The CB and VB of Cu<sub>2</sub>O increase simultaneously as a result of the electron flow. It is acknowledged that the energy levels of the CB minimum (CBM) and the VB maximum (VBM) reflect the reductive ability of electron in CB and oxidative ability of hole in VB<sup>55</sup>. Therefore, it can be inferred that the raised CB and VB of Cu<sub>2</sub>O might enhance the reductive activity of Cu<sub>2</sub>O and weaken its oxidative activity. Without Cu<sub>2</sub>O/Cu contact, the CBM of Cu<sub>2</sub>O ( $-3.2$  eV, vs. AVS) was lower than the LUMO of TCS ( $-3.08$  eV, detail calculation see *Supplementary Information*), thus the Cu<sub>2</sub>O were unable to reduce TCS efficiently. When the Au, Cu<sub>2</sub>O, and Cu contact each other, the CBM of Cu<sub>2</sub>O rise to  $-2.81$  eV. The value is higher than the LUMO of TCS, enabling photo-generated electron transfer from the CB of Cu<sub>2</sub>O to the surface of Au, leading to the reduction of TCS.

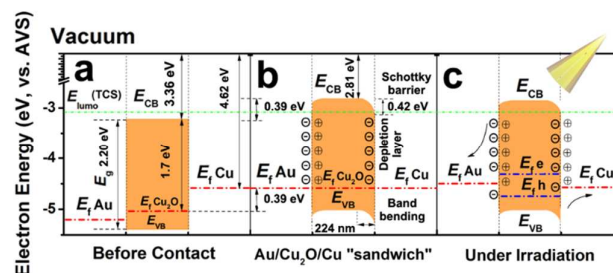


**Figure 5.** Energy levels of Au, Cu<sub>2</sub>O and Cu before contact (a); energy levels and charge separation of Au/Cu<sub>2</sub>O/Cu “sandwich” like structure in dark (b) and under light irradiation (c).

From another side, the Schottky junction between Au/Cu<sub>2</sub>O interfaces plays an important role in the charge separation under light excitation. The Schottky junctions build up an internal electric field which accelerates the electrons and holes to move in the opposite direction once they are generated inside or near the Schottky junction. That is to say, the metal part becomes a fast lane for charge transfer and its surface acts as a charge-trap center to accommodate more photoreactions. The Schottky junction and the fast charge transfer effectively suppress the electron-hole recombination.

Because Cu<sub>2</sub>O is a p-type semiconductor, with holes as majority carriers, the accumulation of holes will cause serious photo-etching.<sup>31</sup> That is, the photo-generated holes are easy to accumulate in the space charge region, leading to the crystalline instability and oxidation of Cu<sub>2</sub>O to CuO. However, little such oxidation was detected on the Au-Cu<sub>2</sub>O NWAs after 16 runs of photocatalytic experiments (as evidenced by the

Fig. S4†, XRD analysis). The unusual photostability of Au-Cu<sub>2</sub>O NWAs can also be attributed to the Au/Cu<sub>2</sub>O/Cu “sandwich” like structure (Fig. 5c). Under light irradiation, the photo-generated electrons and holes split the Fermi energy level of Cu<sub>2</sub>O into a higher electron Fermi energy level ( $E_F$ , e<sup>-</sup>) and lower hole Fermi energy level ( $E_F$ , h<sup>+</sup>).<sup>59</sup> Driven by the internal electronic field, the photo-generated electrons migrate to the Au/Cu<sub>2</sub>O side and react with adsorbed TCS; while the photo-generated holes transfer to Cu<sub>2</sub>O/Cu side and are consumed by recombining with the electrons on the Cu<sub>2</sub>O/Cu side. As a sequence, the holes will not anymore accumulate in the VB of Cu<sub>2</sub>O. Therefore, the photo-etching of holes are eliminated, which give rise to the favorable stability of Au-Cu<sub>2</sub>O NWAs.

#### 4. Conclusions

In summary, Au-Cu<sub>2</sub>O NWAs was prepared by beam sputtering Au onto Cu<sub>2</sub>O nanowires grown from a Cu foil. When Au-Cu<sub>2</sub>O NWAs was applied to degrade TCS in aqueous solution as a photocatalyst, it showed enhanced photoabsorptivity, photocatalytic activity, and photostability under visible light irradiation. The degradation of TCS was mainly ascribed to the photocatalytic reduction by Au-Cu<sub>2</sub>O NWAs which bring about less toxic by-products and high dechlorination efficiency. The performance of Au-Cu<sub>2</sub>O NWAs can be attributed to the Au/Cu<sub>2</sub>O/Cu “sandwich” structure. Taking advantage of the structure, the energy band of Cu<sub>2</sub>O was modified: the photo-generated electrons in CB were reinforced, while the photo-generated holes in VB were eliminated. To the best of our knowledge, the photocatalytic reduction of TCS and “sandwich” structure of Au-Cu<sub>2</sub>O NWAs have not been reported previously. Moreover, Au-Cu<sub>2</sub>O NWAs is suitable to large-scale commercial production due to abundant raw material sources, simple producing technique and low production cost. We will continue to advance the practical application of Au-Cu<sub>2</sub>O NWAs and hope its wide application in the future.

#### Acknowledgements

This work was supported by National Natural Science Foundation of China (Project 21207004), Beijing Natural Science Foundation (8142025), Specialized Research Fund for the Doctoral Program of Higher Education (Project 20120003120027), Special Funds of State Key Joint Laboratory of Environment Simulation and Pollution Control (11Y06ESPCN) and the Fundamental Research Funds for the Central Universities (2012LYB10). We also acknowledge financial support from the Brook Byers Institute for Sustainable Systems, Hightower Chair, and the Georgia Research Alliance at Georgia Tech.

#### References

- 1 E. Engelhaupt, *Environ. Sci. Technol.*, 2007, **41**, 2072–2072.
- 2 A. L. Perez, M. A. De Saylor, A. J. Slocombe, M. G. Lew, K. M. Unice and E. P. Donovan, *Environ. Toxicol. Chem.*, 2013, **32**, 1479–1487.

- 3 B. Wilson, R. F. Chen, M. Cantwell, A. Gontz, J. Zhu and C. R. Olsen, *Mar. Pollut. Bull.*, 2009, **59**, 207–212.
- 4 P. Gautam, J. S. Carsella and C. A. Kinney, *Water Res.*, 2014, **48**, 247–256.
- 5 A. Binelli, M. Parolini, A. Pedriali and A. Provini, *Water Air Soil Pollut.*, 2011, **217**, 421–430.
- 6 P. Martinez Paz, M. Morales, J. L. Martinez Guitarte and G. Morcillo, *Mutat. Res. Genet. Toxicol. Environ. Mutagen.*, 2013, **758**, 41–47.
- 7 J. W. Kim, H. Ishibashi, R. Yamauchi, N. Ichikawa, Y. Takao, M. Hirano, M. Koga and K. Arizono, *J. Toxicol. Sci.*, 2009, **34**, 227–232.
- 8 Triclosan Facts, [http://www.epa.gov/oppsrrd1/REDS/factsheets/triclosan\\_fs.htm](http://www.epa.gov/oppsrrd1/REDS/factsheets/triclosan_fs.htm)
- 9 FDA agrees to set regulation on toxic triclosan, <http://saferchemicals.org/2013/12/12/fda-agrees-to-set-regulation-on-toxic-triclosan/>.
- 10 J. Heidler and R. U. Halden, *Chemosphere*, 2007, **66**, 362–369.
- 11 T. A. Ternes, M. Meisenheimer, D. McDowell, F. Sacher, H. J. Brauch, B. H. Gulde, G. Preuss, U. Wilme and N. Z. Seibert, *Environ. Sci. Technol.*, 2002, **36**, 3855–3863.
- 12 A. Butkovskiy, A. W. Jeremiasse, L. H. Leal, T. van der Zande, H. Rijnaarts and G. Zeeman, *Environ. Sci. Technol.*, 2014, **48**, 1893–1901.
- 13 T. Methatham, M. C. Lu and C. Ratanatamskul, *Desalin. Water Treat.*, 2014, **52**, 920–928.
- 14 M. J. M. de Vidales, C. Saez, P. Canizares and M. A. Rodrigo, *J. Chem. Technol. Biotechnol.*, 2013, **88**, 823–828.
- 15 K. L. Rule, V. R. Ebbett and P. J. Vikesland, *Environ. Sci. Technol.*, 2005, **39**, 3176–3185.
- 16 H. S. Son, G. Ko and K. D. Zoh, *J. Hazard. Mater.*, 2009, **166**, 954–960.
- 17 K. Sankoda, H. Matsuo, M. Ito, K. Nomiya, K. Arizono and R. Shinohara, *Bull. Environ. Contam. Toxicol.*, 2011, **86**, 470–475.
- 18 M. Mezcua, M. J. Gomez, I. Ferrer, A. Aguera, M. D. Hernando and A. R. Fernandez-Alba, *Anal. Chim. Acta* 2004, **524**, 241–247.
- 19 M. Pelaez, N. T. Nolan, S. C. Pillai, M. K. Seery, P. Falaras, A. G. Kontos, P. S. M. Dunlop, J. W. J. Hamilton, J. A. Byrne, K. O'Shea, M. H. Entezari and D. D. Dionysiou, *Appl. Catal. B-Environ.*, 2012, **125**, 331–349.
- 20 J. An and Q. Zhou, *J. Environ. Sci.*, 2012, **24**, 827–833.
- 21 P. D. Tran, S. K. Batabyal, S. S. Pramana, J. Barber, L. H. Wong and S. C. J. Loo, *Nanoscale*, 2012, **4**, 3875–3878.
- 22 X. Li, J. G. Yu, J. X. Low, Y. P. Fang, J. Xiao and X. B. Chen, *J. Mater. Chem. A*, 2015, **3**, 2485–2534.
- 23 E. Pastor, F. M. Pesci, A. Reynal, A. D. Handoko, M. J. Guo, X. Q. An, A. J. Cowan, D. R. Klug, J. R. Durrant and J. W. Tang, *Phys. Chem. Chem. Phys.*, 2014, **16**, 5922–5926.
- 24 H. L. Li, Y. G. Lei, Y. Huang, Y. P. Fang, Y. H. Xu, L. Zhu and X. Li, *J. Nat. Gas Chem.*, 2011, **20**, 145–150.
- 25 X. Li, J. Q. Wen, J. X. Low, Y. P. Fang and J. G. Yu, *Sci. Chin. Mater.*, 2014, **57**, 70–100.
- 26 Y. Xu, H. Wang, Y. F. Yu, L. Tian, W. W. Zhao and B. Zhang, *J. Phys. Chem. C*, 2011, **115**, 15288–15296.
- 27 H. Y. Jing, T. Wen, C. M. Fan, G. Q. Gao, S. L. Zhong and A. W. Xu, *J. Mater. Chem. A*, 2014, **2**, 14563–14570.
- 28 H. G. Yu, J. G. Yu, S. W. Liu and S. Mann, *Chem. Mater.*, 2007, **19**, 4327–4334.
- 29 Y. G. Zhang, L. L. Ma, J. L. Li and Y. Yu, *Environ. Sci. Technol.*, 2007, **41**, 6264–6269.
- 30 L. I. Bendavid, Ph.D. Dissertation, Ph.D. Dissertation, Princeton University, 2013.

- 31 T. Mahalingam, J. S. P. Chitra, J. P. Chu, H. Moon, H. J. Kwon and Y. D. Kim, *J. Mater. Sci. - Mater. Electron.*, 2006, **17**, 519–523.
- 32 P. Christopher, H. L. Xin and S. Linic, *Nat. Chem.*, 2011, **3**, 467–472.
- 33 L. Zhang, D. A. Blom and H. Wang, *Chem. Mater.*, 2011, **23**, 4587–4598.
- 34 Y. L. Pan, S. Z. Deng, L. Polavarapu, N. Y. Gao, P. Y. Yuan, C. H. Sow and Q. H. Xu, *Langmuir*, 2012, **28**, 12304–12310.
- 35 Y. Yue, M. Chen, Y. Ju and L. Zhang, *Scr. Mater.*, 2012, **66**, 81–84.
- 36 X. C. Jiang, T. Herricks and Y. N. Xia, *Nano Lett.*, 2002, **2**, 1333–1338.
- 37 P. Wang, Y. H. Ng and R. Amal, *Nanoscale*, 2013, **5**, 2952–2958.
- 38 D. B. Wang, M. S. Mo, D. B. Yu, L. Q. Xu, F. Q. Li and Y. T. Qian, *Cryst. Growth Des.*, 2003, **3**, 717–720.
- 39 H. Solache-Carranco, G. Juárez-Díaz, J. Martínez-Juárez and R. Peña-Sierra, *Rev. Mex. Fis.*, 2009, **55**, 393.
- 40 L. Kong, W. Chen, D. Ma, Y. Yang, S. Liu and S. Huang, *J. Mater. Chem.*, 2012, **22**, 719–724.
- 41 G. Vincent, A. Aluculesei, A. Parker, C. Fittschen, O. Zahraa and P. M. Marquaire, *J. Phys. Chem. C*, 2008, **112**, 9115–9119.
- 42 Y. Nosaka, T. Daimon, A. Y. Nosaka and Y. Murakami, *Phys. Chem. Chem. Phys.*, 2004, **6**, 2917–2918.
- 43 D. Kim, J. Lee, J. Ryu, K. Kim and W. Choi, *Environ. Sci. Technol.*, 2014, **48**, 4030–4037.
- 44 J. Staehelin and J. Hoigne, *Environ. Sci. Technol.*, 1985, **19**, 1206–1213.
- 45 K. D. Pickering and M. R. Wiesner, *Environ. Sci. Technol.*, 2005, **39**, 1359–1365.
- 46 C. Santaella, B. Allainmat, F. Simonet, C. Chaneac, J. Labille, M. Auffan, J. Rose and W. Achouak, *Environ. Sci. Technol.*, 2014, **48**, 5245–5253.
- 47 S. Garg, C. Jiang, C. J. Miller, A. L. Rose and T. D. Waite, *Environ. Sci. Technol.*, 2013, **47**, 9190–9197.
- 48 H. Fakhouri, J. Pulpytel, W. Smith, A. Zolfaghari, H. R. Mortaheb, F. Meshkini, R. Jafari, E. Sutter and F. Arefi Khonsari, *Appl. Catal. B-Environ.*, 2014, **144**, 12–21.
- 49 J. C. Yu, T. Y. Kwong, Q. Luo and Z. Cai, *Chemosphere*, 2006, **65**, 390–399.
- 50 V. Bokare, K. Murugesan, Y. M. Kim, J. R. Jeon, E. J. Kim and Y. S. Chang, *Bioresour. Technol.*, 2010, **101**, 6354–6360.
- 51 K. Aranami and J. W. Readman, *Chemosphere*, 2007, **66**, 1052–1056.
- 52 L. Sanchez-Prado, M. Llompарт, M. Lores, C. Garcia-Jares, J. M. Bayona and R. Cela, *Chemosphere*, 2006, **65**, 1338–1347.
- 53 C. Tixier, H. P. Singer, S. Canonica and S. R. Müller, *Environ. Sci. Technol.*, 2002, **36**, 3482–3489.
- 54 H. J. Liu, X. L. Cao, G. G. Liu, Y. L. Wang, N. Zhang, T. Li and R. Tough, *Chemosphere*, 2013, **93**, 160–165.
- 55 N. Serpone and E. Pelizzetti, *Photocatalysis: fundamentals and applications*, Wiley, 1989.
- 56 A. V. Walker and J. T. Yates, *J. Phys. Chem. B*, 2000, **104**, 9038–9043.
- 57 S. Kim, M. Song and S. Rhee, *ECS Trans.*, 2008, **16**, 355–362.
- 58 D. Cahen and A. Kahn, *Adv. Mater.*, 2003, **15**, 271–277.
- 59 A. L. Linsebigler, G. Lu and J. T. Yates, *Chem. Rev.*, 1995, **95**, 735–758.